Comparison of a dyadic wavelet image enhancement algorithm with unsharp masking and median filtering for mammography

Yunong Xing, Walter Huda, Andrew Laine,
Jian Fan, Barbara Steinbach, Janice Honeyman

University of Florida, Department of Radiology
Box 100374, Gainesville, FL 32610-0374

ABSTRACT

Image processing techniques using wavelet signal analysis techniques have shown promise in mammography. Wavelet algorithms are compared with traditional image enhancement techniques of unsharp masking and median filtering. Computer simulated phantom images were generated containing lesions mimicking masses and microcalcifications. The degree of image enhancement was evaluated by comparing processed and original signal-to-noise (SNR) ratios in such phantom images. Results obtained in this study suggest that image processing algorithms based on the wavelet transform are likely to enhance the visibility of low-contrast features in mammograms.

Keywords: Image processing, wavelets, unsharp masking, median filtering, mammography, masses, microcalcifications, imaging performance

1. INTRODUCTION

A novel approach to image processing in mammography has been based on algorithms of the wavelet transform.[1,2,3] In general, wavelet algorithms possess several free parameters, and understanding the importance of each of these parameters is of benefit.[4] In this paper, computer generated phantom images simulating masses and microcalcifications were used. The ratio of output-to-input SNR ratios was the descriptor used to assess algorithm performance. Use of this procedure permitted the free parameters for any image processing algorithm to be investigated and optimized. Three image processing algorithms were evaluated in this study: (i) an algorithm based on the dyadic wavelet transform; (ii) unsharp masking; and (iii) median filtering.

2. METHOD

2.1. Mathematical phantom design

Computer simulated phantoms shown in Fig. 1 consisted of 512^2 image matrices with 8 bits per pixel (≡ 256 gray levels). The phantom was divided into 25 equal squares (i.e., a 5 x 5 grid) with each region having 100^2 pixels. Five randomly selected squares contained a mass and five contained a single microcalcification. The mass was modelled as a sphere with a radius of 30 pixels and signal intensity (in gray level) corresponded to the thickness of the sphere (i.e., the peak of the sphere signal had a gray level of 60 above background). Each microcalcification was a 3 x 3 square with a gray level of 30 above background. Pseudo-random gaussian white noise, with a standard deviation σ = 10, was obtained using the Matlab software package (The Mathworks Inc., Natick, MA) and was added to each of the 25 distinct regions. The background had an average gray level value of 128.

2.2. Processing algorithms

2.2.1. Dyadic transform

The algorithm evaluated in this study is based on a dyadic transform [2] which permits a perfect reconstruction of an original image. The inner product of a signal (S) with a wavelet (ϕ) reflects the character of S within the time-frequency region where ϕ is localized. Provided ϕ is spatially localized, two-dimensional features such as shape and orientation will be preserved in transform space and can thus be used to characterize these features through scale space.

 0-8194-1782-3/95/$6.00

A multiresolution representation divides the frequency spectrum of an image x into a low-pass sub-band image y_o^L and a set of band-pass sub-band images y_j^i, i=1, ... N and j=1, ... M, where N and M denote the number of levels and orientations for a representation, respectively. If F_j^i is the equivalent filter for the ith level and jth channel, $W_{ij}[x]$ denotes the operation of filtering x. A sub-band image of an N-level multiresolution decomposition is then given by

$$y_j^i = W_{ij}[x] . \quad (1)$$

The two-dimensional dyadic wavelet transform results in a multiresolution representation, which partitions orientations into two bands (i.e., M = 2), corresponding to horizontal and vertical bands.[3,5] At each level L, two-dimensional wavelet maxima coefficients were determined. Values of wavelet coefficients above some threshold T were multiplied by a gain factor, G, followed by the inverse Wavelet Transform to generate a processed image.

There were three parameters to select for our image processing algorithm: (1) a *single* selected level (L = 1 through L = 8) at which modifications to wavelet coefficients were performed with L = 1, corresponding to the highest spatial frequencies, and L = 8 to the lowest (i.e., the DC cap); (2) the threshold value T above which wavelet coefficients were modified; and (3) the gain factor G by which selected wavelet coefficients (i.e., those above threshold T) were multiplied prior to performing the inverse transform.

2.2.2. Unsharp masking

Unsharp masking[6] consisted of three steps. First, an original image I(x,y) was blurred by convolving it with a mask image M(x,y) to obtain a blurred image B(x,y). A difference image D(x,y) was obtained by subtracting B(x,y) from I(x,y). The processed image O(x,y) was then obtained by adding the weighted difference image W x D(x,y) to the original image I(x,y). Mathematically, this can be written as

$$O(x,y) = I(x,y) + W \cdot [I(x,y) - I(x,y) \bigstar B(x,y)] \quad (2)$$

The mask image M(x,y) is normally rectangular in shape, and its size may be selected. As a result, unsharp masking has two free parameters: the kernel size and the degree of enhancement represented by the term W.

2.2.3. Median filtering

The median filtering technique is a nonlinear process useful in reducing impulsive noise.[7] A two-dimensional window is moved across the image, and the median intensity value of the pixels within this window is selected as the output intensity of the pixel being processed. The window is usually rectangular in shape, of size M x M. Thus for median filtering there was only one free parameter for the window size M.

2.3. Evaluation parameters

The signal strength, S, in the simulated phantom images was defined as

$$S = \frac{1}{5} \cdot \sum_{j=1}^{j=5} (S_j - B_j) \quad (3)$$

where S_j was the gross counts within the jth region with a signal summed over a central area containing the signal, and B_j was the corresponding gross counts in the adjacent region without the signal. The noise, N, in the simulated phantom image was then formulated as

$$N = \frac{1}{5} \cdot \sum_{j=1}^{j=5} \sigma_{B_j} \quad (4)$$

where σ_{Bj} is the standard deviation in the central region of the jth square which does *not* contain a signal. The definitions for signal and noise were used to obtain an input SNR ratio (SNR_I) and the corresponding value of the output SNR ratio (SNR_o) in the processed image. The resultant enhancement factor, EF, was then computed by the expression

$$EF = \frac{SNR_o}{SNR_i} \quad (5)$$

Five regions contained a mass and five regions contained a single microcalcification feature. As a result, for each signal there were a total of five independent measurements, permitting a mean (± one standard deviation) of the EF parameter to be computed. Standard deviations of the computed EF parameter are shown in the figures as vertical error bars.

The EF computed in this study has been shown to have an excellent correlation with the results of psychophysical perception experiments for simple features embedded in white noise.[8] Accordingly, any increase in the EF obtained with an image processing algorithm can be claimed to result in an improvement in the visibility of a feature.

3. RESULTS AND DISCUSSION

3.1. Dyadic transform

Each phantom was processed with threshold, T, and gain, G, fixed at values 0.25 and 30, respectively, to find the optimal level for each distinct signal. Fig. 2 shows how the EF varied with the L parameter for both microcalcifications and masses. These data indicate that the optimal value of L depends on the size of the feature of interest and was "2" for microcalcification and "5" for mass. The lowest level (L = 1) corresponded to higher spatial frequencies. Therefore, an optimal level for small objects (microcalcifications) is lower than that for large objects (masses). For high levels (L = 8 for masses and L = 5 to 8 for microcalcifications) corresponding to low-spatial frequencies, there was no significant enhancement of either the signal or the noise, and the resultant value of EF 1.0 was observed.

Each phantom was subsequently processed at the optimal level to investigate the significance of the threshold (T) parameter. Threshold values investigated were 1, 2, 4, 8, 16, 32, 64, and 128. Fig. 3 shows how the EF varied with each threshold parameter. We observed that EF fell to unity at the highest threshold values for each type of mammographic feature. This is expected since a high threshold results in no amplification of any wavelet coefficients, and the processed image is identical to its original (i.e., EF is equal to 1). As the threshold was reduced, the EF curve was seen to increase to a constant value, higher than unity, indicating an improvement in imaging performance. For the purpose of investigating the G parameter, (optimal) thresholds values were arbitrarily taken to be 1 and 4 for masses and microcalcifications, respectively.

Each phantom was subsequently processed at an optimal value of level (L) and threshold (T) to determine the dependence of EF on the G parameter. Gain values investigated were 5, 10, 20, 40, 80, and 160. The results are shown in Fig. 4 for both mammographic features. We observed that EF showed a monotonic increase with the G parameter. The highest EF values

obtained were of the order of 3, which suggest a large improvement in feature visibility. It is important to note, however, that the use of a high gain factor may result in the detection of false-positives, which should be taken into account when evaluating any image enhancement scheme.[8]

3.2. Unsharp masking

The phantom was processed with kernel sizes of 3, 5, 11, 21, 41, 81 and W values of 1, 2, 5, 10. For both mammographic features, the results are shown in Fig. 5 and indicate similar trends. The EF was always smaller than unity, showing that this approach does not improve the SNR ratio of the specific objects used in this phantom. The basic reason for this is that unsharp masking is effectively a high-pass filtering operation. The blurred image B(x,y) is a low-pass version of the original image, and the difference image D(x,y) is a high-pass version of the original image. The weighted high-pass component of the original image W x D(x,y) was added back to the original image to obtain the processed image (see equation 2). The signal is located in the low-spatial frequency range, but the (white) noise dominates the high-spatial frequency region; therefore, EF was always smaller than unity using unsharp masking.

As the kernel size increased, EF increase was asymptote to unity as shown in Fig. 5. This is because with a larger kernel, the blurred image B(x,y) is closer to the original image I(x,y), and the difference image D(x,y) is closer to zero; therefore, the processed image O(x,y) is closer to the original image I(x,y), resulting in an EF value close to unity. As shown in Fig. 5, the larger the multiplying factor W, the lower the resultant EF. This is because as W increased, more of the noise which dominates the high-spatial frequency was added to the original image, decreasing the resultant EF.

It has been reported that the detectability of simple patterns *can* be increased using unsharp masking.[6] The study by Loo *et al* showed that small kernel size degraded signal detectability, and that with larger weighting factors worse SNR ratios were obtained. The trends reported by these authors were generally similar to the findings of this study. The reported improvement in image SNR of processed images appears to contradict the result presented in Fig. 5. Upon closer inspection, however, there is no conflict. Improvements in observer SNR ratios reported by Loo *et al* were only obtained when the *internal* noise of the observers was taken into account.[6] This feature was not incorporated in this study since the primary goal was to compare the intrinsic properties of each image processing algorithm. In practice, the use of simple window and level features when displaying a digital image may be used to overcome the internal noise of an observer.

3.3. Median filtering

Fig. 6 shows how the EF parameter varies with kernel size, M, of the median filter. Median filtering is a low-pass filtering operation, so for large features (masses), high EF values can be attained. For masses, EF values as high as 16 were achieved. For kernel sizes larger than the signal, the EF was reduced because of a blurring of the signal at the edges. For the small sized microcalcification in this phantom (3 x 3 pixels), the EF was above unity for smaller kernel sizes and below unity for larger sizes as shown in Fig. 6. The value of EF for the largest kernel size (81) was actually negative, indicating that random fluctuation in the neighboring noise-only square was larger than that of the processed microcalcification area.

It is important to note that the use of median filtering reduces resolution and is designed solely to reduce image noise with no inherent ability to enhance the features of interest in mammograms.[9] Although the results obtained in this study appear to be very promising, real mammograms are far more complex than the kind of signal buried in white noise used in this study. In practice, it is likely that mammograms could be processed to reduce image noise (denoising) prior to the application of a wavelet based algorithm to enhance the visibility of selected types of low-contrast features. Given the multiscale capability of any wavelet decomposition scheme, these features may be incorporated into a single algorithm. Thus, despite the apparent promise of the results shown in Fig. 6, it is more likely that a wavelet based approach to the processing of mammograms will result in superior clinical performance.

4. CONCLUSIONS

1. Computed Enhancement Factor (EF) showed that the dyadic wavelet algorithm can significantly improve the visibility of features such as masses and microcalcifications embedded in pseudo-random noise.

2. The multiscale capabilities of a wavelet signal decomposition offers possibilities of enhancing selected features and reducing noise simultaneously.

3. Unsharp masking amplifies the noise in the high-frequency range and reduces the SNR in processed images for simple features masked with white noise.

4. Unsharp masking improved the visibility of low-contrast signals only when the internal noise of a human observer was taken into account.

5. For simple features buried in white noise, a median filter improved SNR as a result of reducing image noise, but degraded SNR with kernel sizes larger than the signal.

5. ACKNOWLEDGEMENTS

Technical support by Sergio Schuler, Yisheng Zheng and Zhenxue Jing is gratefully acknowledged. Editorial assistance by Linda Waters-Funk is also appreciated.

This work was sponsored in part by the Whitaker Foundation and the U.S. Army Medical Research and Development Command, Grant No. DAMD17-93-J-3003.

6. REFERENCES

1. Laine A and Song S. "Wavelet processing techniques for digital mammography," *Proceedings of SPIE: Conference on Visualization in Biomedical Computing*, SPIE, Vol. 1808, pp. 610-624, 1992.

2. Laine A, Song S, Fan J, Huda W, Honeyman J, Steinbach B. "Adaptive multiscale processing for contrast enhancement," *Proceedings of the SPIE (San Jose)*, SPIE, Vol. 1905, pp. 521-532, 1993.

3. Laine AF, Schuler S, Fan J, Huda W. "Mammographic feature enhancement by multiscale analysis," *IEEE Trans. on Med. Imaging*, Vol. 13, pp. 725-740, Dec. 1994.

4. Jing Z, Zheng Y, Huda W, Laine A, Fan J, Xing Y. "Quantitative evaluation of wavelet based image processing algorithms," *Proceedings of SPIE: Conference on Wavelet Applications in Signal and Image Processing II*, SPIE, Vol. 2303, pp. 569-578, 1994.

5. Daubechies I. Ten Lectures on Wavelets, *Society for Industrial and Applied Mathematics*, Philadelphia, PA, 1992.

6. Loo L-ND, Doi K, Metz CE. "Investigation of basic imaging properties in digital radiography. 4. Effect of unsharp masking on the detectability of simple patterns," *Med. Phys.*, Vol. 12, pp. 209-214, Mar./Apr. 1985.

7. Lim JS. *Two-Dimensional Signal and Image Processing*, Prentice Hall, Englewood Cliffs NJ, 1990.

8. Xing Y, Huda W, Laine A, Fan J. "Simulated phantom images for optimizing wavelet based image processing algorithms in mammography," *Proceedings of SPIE: Conference on Mathematical Methods in Medical Imaging III*, SPIE, Vol. 2299, pp. 207-217, 1994.

9. Dhawan AP, Buelloni G, Gordon R. "Enhancement of mammographic features by optimal adaptive neighborhood image processing," *IEEE Trans. on Med. Imaging*, Vol. MI-5, pp. 8-15, 1986.

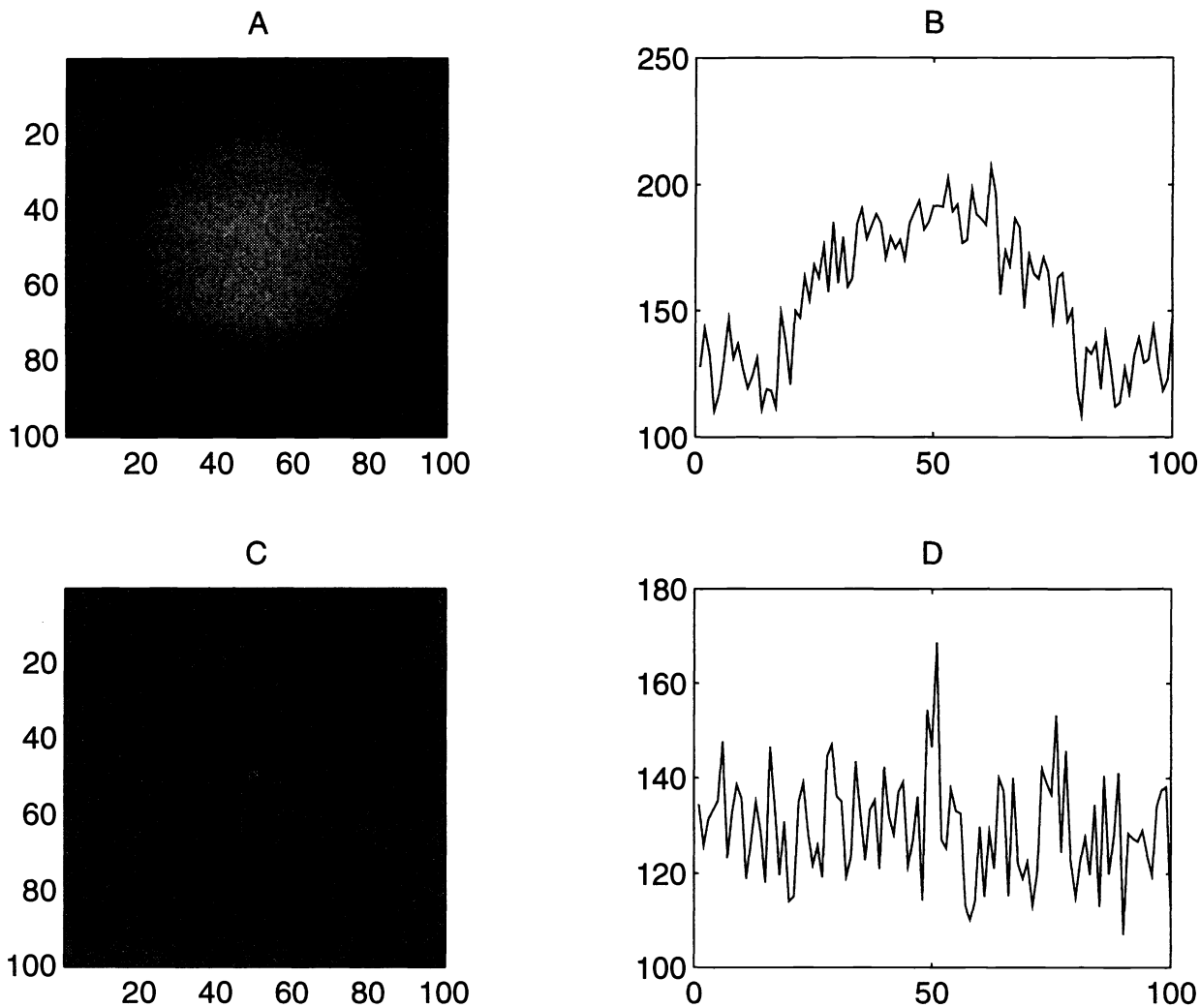

Figure 1
Computer Simulated Phantoms
A) Mass; B) Cetral Profile of Mass;
C) Microcalcification; D) Central Profile of Microcalcification

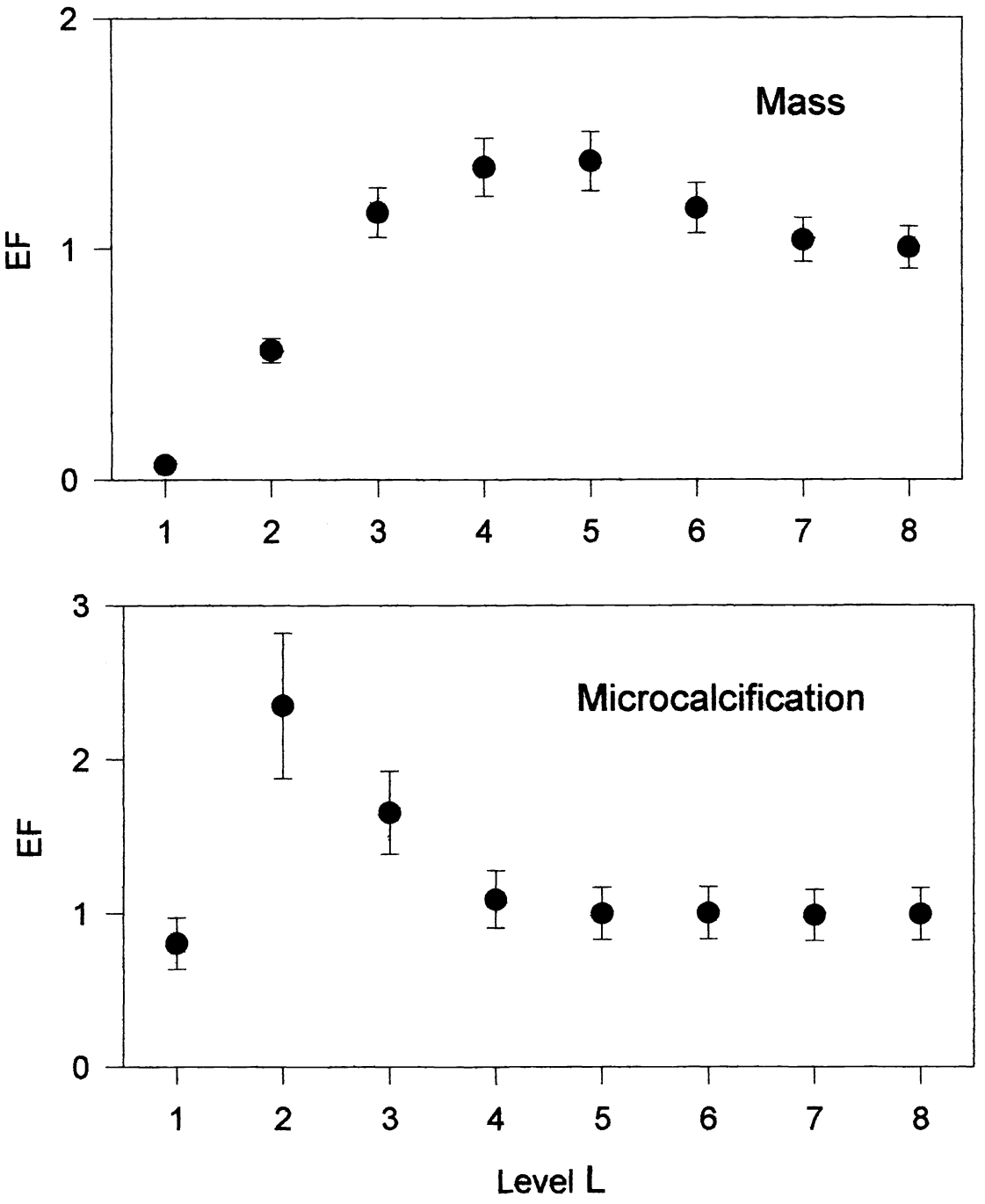

Figure 2

Enhancement factor vs level (L)

Dyadic Wavelet Transform T = 0.25, G = 30

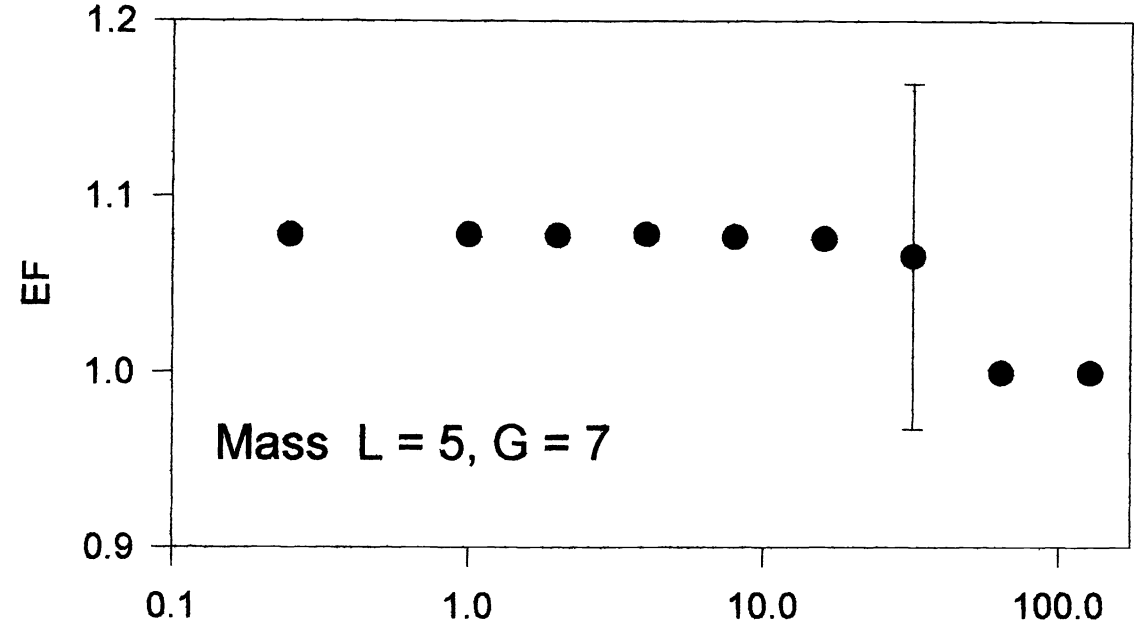

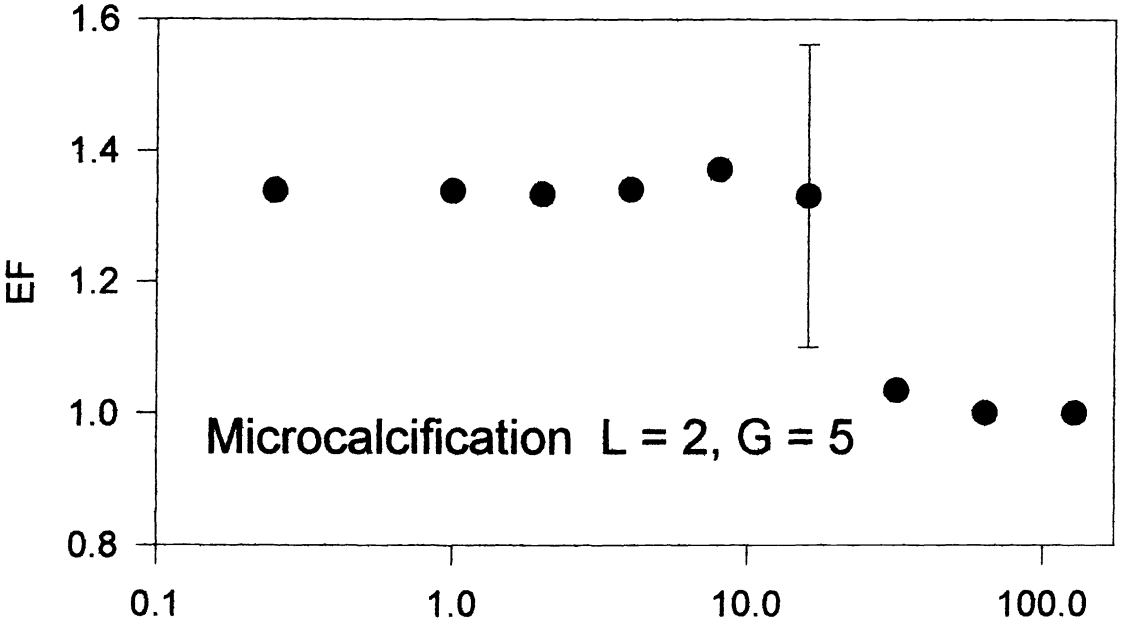

Figure 3

Enhancement factor vs Threshold (T)

Dyadic Wavelet Transform

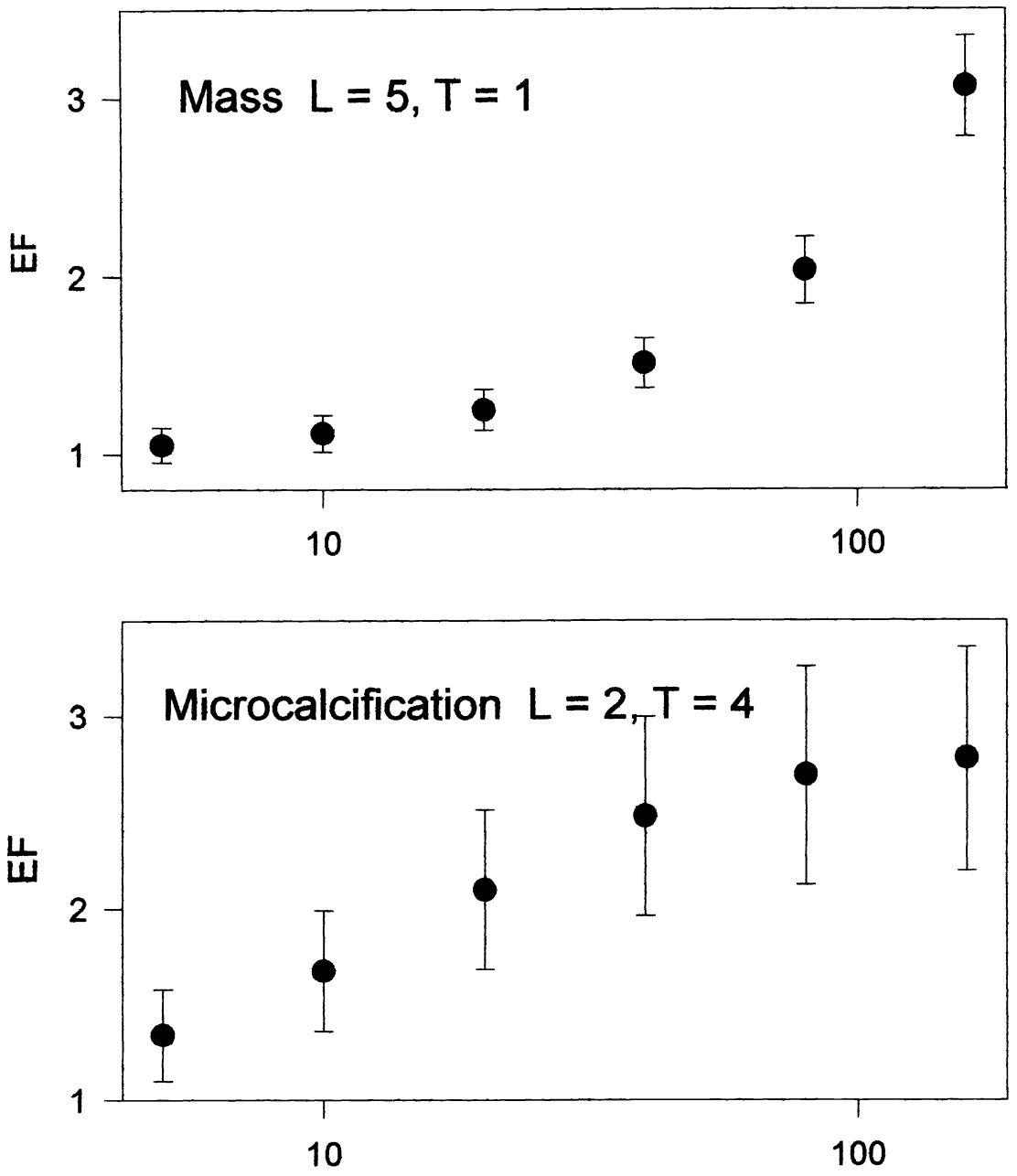

Figure 4

Enhancement factor vs Gain (G)

Dyadic Wavelet Transform

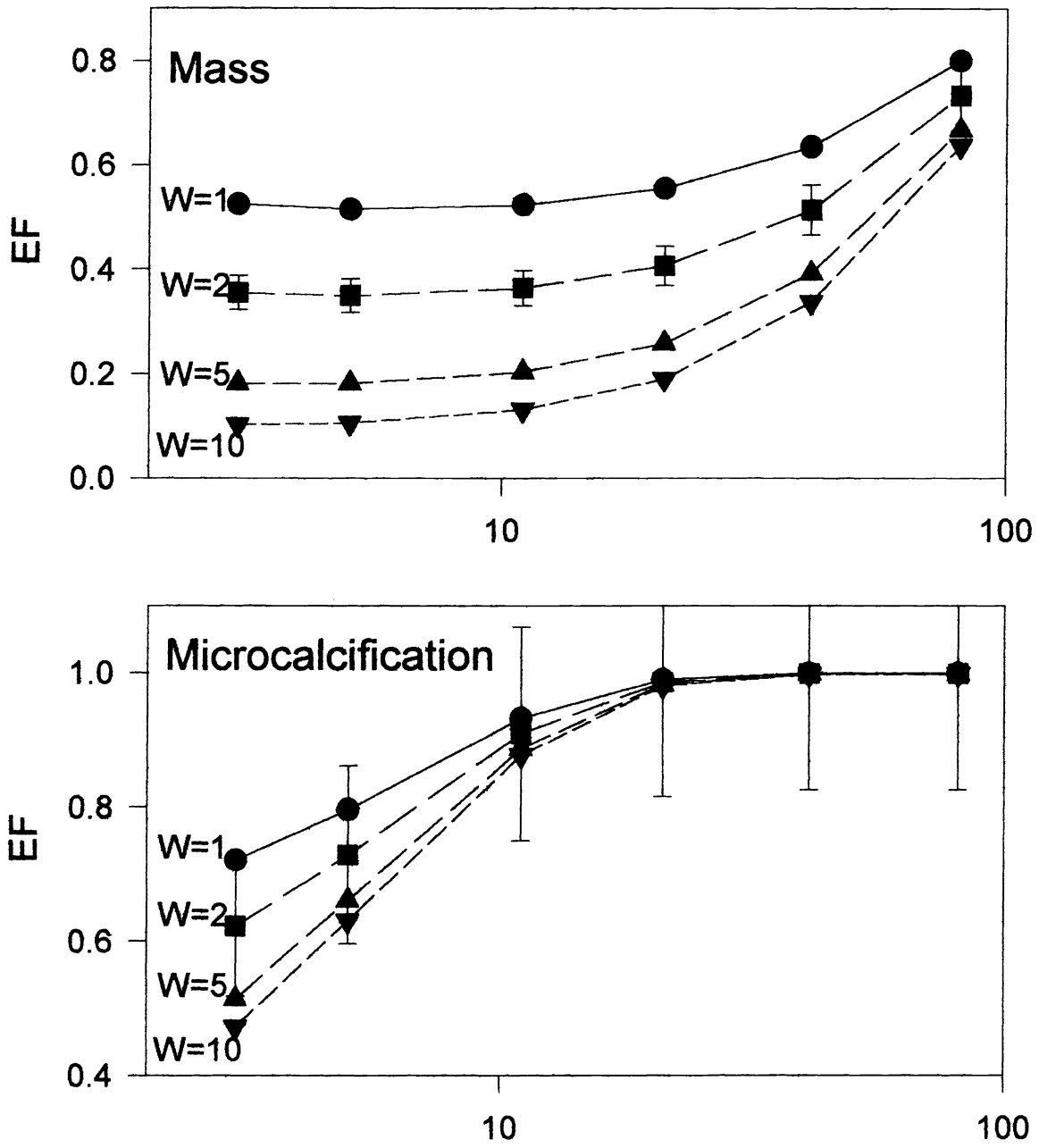

Figure 5

Enhancement factor vs Kernel size and weight W

Unsharp Masking

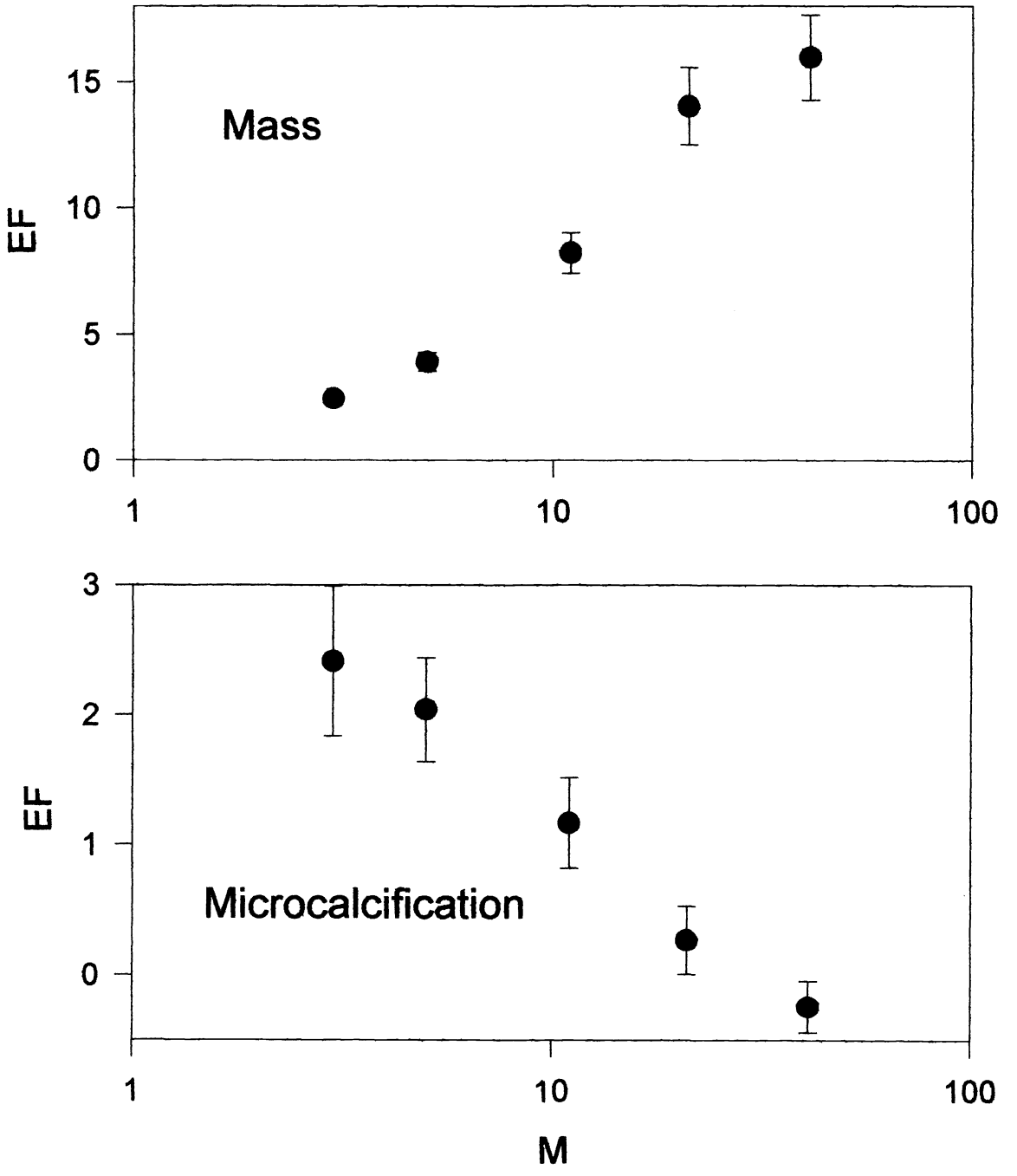

Figure 6

Enhancement factor vs kernel size M

Median Filtering